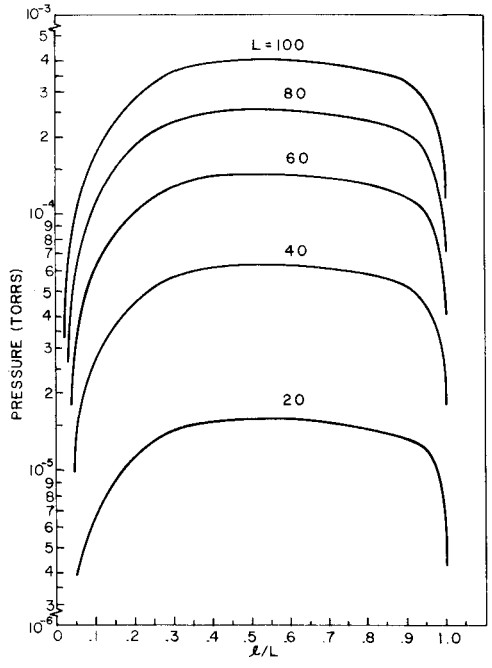

Fig. 1 Pressure distribution in the DAM/B4A composites at 40 min of pumping time (T_o = 300 K, T_w = 20 K, c = 0.015).

It can be seen from Fig. 1 that the pressure increases with the total number of layers of the MLI. For a fixed L, the pressure first increases from the vacuum ambient towards the inner layers, reaches a maximum, then decreases towards the wall. This is because the temperature decreases rapidly near the wall. With the same boundary conditions, results for other values of c can be obtained from Fig. 1 by the multiplication factor $[0.015/(1-0.015)](1-c)/c$.

Since the temperature drops rapidly only near the wall, the maximum pressure in an MLI depends only weakly on T_w. Thus, the maximum pressures shown in Fig. 1 remain roughly the same for the liquid oxygen tanks with a wall temperature of 100 K. Experimental measurements of pressure in a non-isothermal MLI are not available for comparison.

IV. Conclusions

The solution for the outgas dominated pressure distribution in a DAM/B4A multilayer insulation system given by Eq. (13) only applies to the early stage of the diffusion phase of outgassing. However, this stage represents a rather important period of time as the outgassing rate in this period is large, resulting in a high pressure inside the insulation composite. Thus, the pressure prevailing in the MLI in this period can be used as a reference regarding the thermal performance of the insulation composite. At later times when the validity of Eq. (12) no longer holds, further computation of the pressure distribution, if necessary, must be obtained from Eq. (10) by using other realistic $q-T$ relations. As the relaxation time of the gases in the MLI usually is short,[2] the system can be considered "quasi-steady." By using the outgassing rate and boundary conditions at any given time, the problem can be solved as time independent. The solutions for a chosen sequence of time then constitute the solution as function of the time.

The cryopumping effect of the very cold layers near the wall has not been included in this analysis. It should be noted that when cryopumping occurs, the number density decreases near the wall, and the maximum pressure in the MLI is lower than that computed from the present method.

The numerical examples presented are for the MLI composites using double-aluminized Mylars for radiation shields with Dacron net B4A as spacers, as the $q-T$ data for these composites are better known. Since the outgassing rate is a rapidly decreasing function of the time, it can be seen from Fig. 1 that all the composites considered are adequate for long-term space missions. However, from previous experience of Apollo flights, it was learned that aluminized Mylars could not stand moisture and high temperature (considerably exceeding the room temperature). For such environments, goldized Kapton is more suitable for radiation shields.[3] Therefore, further experimental study of the outgassing rates of this and other potential candidate materials is desirable.

References

[1] Glassford, A. P. M., "Outgassing Behavior of Multilayer Insulation Materials," *Journal of Spacecraft and Rockets*, Vol. 7, No. 12, Dec. 1970, pp. 1464–1468.

[2] Lin, J. T., "Analysis of Gas Flow Through a Multilayer Insulation System," *AIAA Journal*, Vol. 11, No. 7, July 1973, pp. 995–1000.

[3] Krause, D. R., "Development of Lightweight Material Composites to Insulate Cryogenic Tanks for 30-Day Storage in Outer Space," Final Rept., NASA Contract NAS8-26006, June 1972, McDonnell Douglas Astronautics Co., Huntington Beach, Calif.

[4] Santeler, D. J., "Outgassing Characteristics of Various Materials," *Transactions of Fifth National Symposium on Vacuum Technology*, Pergamon Press, New York, 1958, pp. 1–8.

[5] Dayton, B. B., "Relations Between Size of Vacuum Chamber, Outgassing Rate and Required Pumping Speed," *Transactions of the Sixth National Symposium on Vacuum Technology*, Pergamon Press, New York, 1959, pp. 101–119.

[6] Abramowitz, M. and Stegun, I. A., "Handbook of Mathematical Functions," AMS 55, National Bureau of Standards, U.S. Government Printing Office, Washington, D.C., 1964, pp. 227–251.

[7] Hastings, C., Jr., "Analytical Approximations," Note 143, *Mathematical Tables and Other Aids to Computation*, Vol. 7, No. 41, 1953, pp. 67–69.

Debris Shielding during High-Speed Erosion

W. G. REINECKE*
Avco Systems Division, Wilmington, Mass.

Nomenclature

B = dimensionless empirical constant
C_J = debris particle drag coefficient
G = ratio of mass eroded to rain mass encountered; the mass loss ratio m/M
G_o = ratio of mass eroded to rain mass reaching surface
G' = drop mass loss ratio
L = rain field length
M = total mass encountered
m = mass eroded
R = body radius
r = drop radius
r' = debris particle radius
U = debris efflux speed
u = body speed
u' = air speed over body
w = rain-field concentration
x = distance along body from stagnation point
δ = debris layer thickness
ε = density ratio
η = modified debris shielding parameter
η' = debris shielding parameter
ρ = ambient air density

Received March 11, 1974; revision received June 6, 1974. This work was supported by the U.S. Air Force Materials Laboratory under Contract F33615-72-C-1306.

Index categories: LV/M Simulation; Hypervelocity Impact; Research Facilities and Instrumentation.

* Senior Consulting Scientist. Associate Fellow AIAA.

ρ_l = drop density
ρ_s = body density
ρ' = shock layer air density
σ = debris layer concentration

EXPERIMENTS in Avco's Rain and Dust Erosion Facility (RADEF)[1] have shown that the erosion suffered by a blunt body traversing a rain field at high speed decreases markedly as the rain field concentration is increased. This phenomenon appears to result from the accumulation in the body stagnation region of water and body material ejecta generated by the drop impacts. This accumulated debris tends to shield the body surface from subsequent impacts. Thus debris shielding can reduce the tip erosion experienced by a body flying through rain (or any other ambient particular, such as ice). An experimental consequence of this fact is that an upper limit is established on the concentration of any laboratory rain field in which data relevant to more tenuous natural rain fields may be obtained. It is the purpose of this Note to develop a theory for the debris shielding phenomenon. Specifically, we wish to calculate the effect of rain concentration upon the erosion mass loss ratio G, the ratio of the mass of body material removed by erosion to the mass of rain encountered.

Consider a flat faced, cylindrical sample, or the stagnation region of a spherical sample tested ballistically for rain erosion as in the RADEF. Assume that rain is hitting the surface of the sample and removing mass in a nearly continuous manner, resulting in an approximately uniformly distributed layer of debris. Let the debris layer have a characteristic thickness δ, a debris concentration σ, and an efflux velocity U as shown in Fig. 1. If during the erosion test the specimen encounters rain mass M and loses mass m, continuity yields

$$m+M = 2\pi R\delta U\sigma L/u \tag{1}$$

where R is the specimen radius, L is the rain field length, u the test speed, and thus L/u is the test duration.

Next consider a raindrop of radius r penetrating the debris layer. Before striking the sample surface, the drop will encounter $\pi r^2\,\delta\sigma$ debris mass, and, by analogy with the mass removal from the test sample itself, will lose $G'\pi r^2\,\delta\sigma$ mass, where G' is a mass loss ratio and is likely dependent upon u. Then at impact upon the specimen surface the mass of the drop will be reduced by the fraction

$$G'\frac{\pi r^2\,\delta\sigma}{\frac{4}{3}\pi r^3\rho_l} = \frac{3}{4}G'\frac{\delta\sigma}{r\rho_l} \tag{2}$$

where ρ_l is the drop density. Thus although the test sample sweeps out a rain mass

$$M = w\pi R^2 L \tag{3}$$

during the test, where w is the liquid water concentration, the amount of mass actually reaching the surface is

$$M(1-\tfrac{3}{4}G'\,\delta\sigma/r\,\rho_l) = w\pi R^2 L(1-\tfrac{3}{4}G'\,\delta\sigma/r\,\rho_l) \tag{4}$$

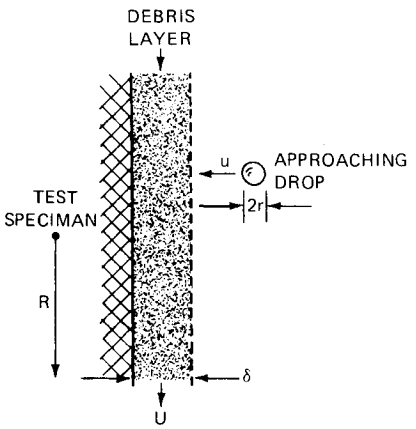

Fig. 1 Sketch of debris layer.

and the mass removed will be

$$m = G_o M(1-\tfrac{3}{4}G'\,\delta\sigma/r\rho_l) \tag{5}$$

where G_o is the ratio of sample mass eroded to the water mass actually striking the surface. Eliminating the product $\delta\sigma$ between Eqs. (1) and (5) solving for m/M yields

$$\frac{m}{M} = G = G_o\frac{1-\frac{3}{8}G'\eta'}{1+\frac{3}{8}G_o G'\eta'} \tag{6}$$

where

$$\eta' = wRu/Ur\,\rho_l \tag{7}$$

and where G is the conventionally defined mass loss ratio, that is, the ratio of sample mass removed to rain mass swept out by the sample in its traversal of the rain field. It is important to note that the value of w in Eq. (7) must be the actual local value of the particle concentration, not a value averaged over a long trajectory made up alternately of locally intense rain fields and large voids.

The quantity R/U in Eq. (7) is the characteristic residence time of a debris particle in the debris layer and can be estimated as follows. Assume that debris particles leave the crater with a zero vectorially averaged velocity component parallel to the sample surface. The particles will then be swept away by aerodynamic forces. It is easy to show that the debris concentration is generally much less than the air density. We also take the local air speed and density to be given by the hypersonic, spherical body approximations

$$\rho' = \rho/\varepsilon \tag{8}$$

and

$$u' = u(x/R)(2\varepsilon)^{1/2} \tag{9}$$

where ρ' and u' are the gas density and speed in the debris (shock) layer, ρ and u are the ambient density and test speed, and x is measured from the model stagnation point. Under these simplifications, an integration of Newton's Second Law for a debris particle originating near the model stagnation point yields

$$R/U = (2\rho_s r'R/\rho u^2 C_D)^{1/2} \tag{10}$$

where r' is a characteristic debris particle radius, ρ_s is the debris particle density, and C_D is the particle drag coefficient. Using Eq. (10) to eliminate R/U from Eq. (7) results in

$$\eta' = \left(2\frac{w^2}{\rho_l^2}\frac{\rho_s r'R}{\rho r^2 C_D}\right)^{1/2} \tag{11}$$

This equation and Eq. (6) represent the solution to the debris shielding problem. It follows that G is an increasing function of the ambient air density ρ, all other test parameters being constant.

We now make an order of magnitude estimate of the size of debris shielding effects. For this purpose take

C_D = 0.4 (an estimate)
ρ_s = 1.7 G/cc (a reinforced plastic)
ρ_l = 1.0 G/cc (water)
r'/r = 0.1 (an estimate)
r/R = 0.1 (a typical value)
ρ = 1.225×10^{-3} G/cc (1 atm)
G' = G_o = 50 (an estimate for u = 14,000 fps)

Then from Eq. (11) η' equals 0.00108 and 0.01157 for w equal to 13 and 139 G/M^3, respectively, and from Eq. (6)

$$G(w = 139)/G(w = 13) = 0.1 \tag{12}$$

From the RADEF data on a reinforced phenolic at 90° impact in rain at 14,000 fps

$$G(w = 139)/G(w = 13) = 0.16 \tag{13}$$

Thus, even with the rough estimates used for r'/r, G', and G_o, it is clear that the theory resulting in Eqs. (6) and (11) does indeed correctly estimate the order of magnitude of debris shielding. Also, note that even for values of G' as great as 100, the quantity $3G'\eta'/8$ is always much less than one (except in very dense rain fields) and can be neglected in the numerator of Eq. (6).

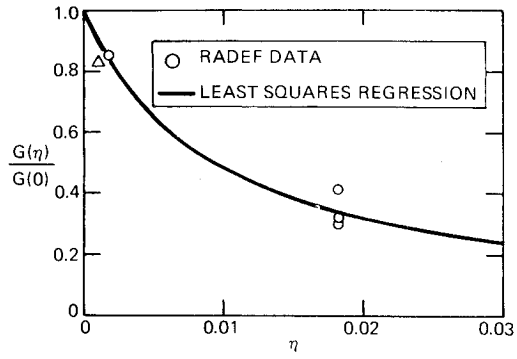

Fig. 2 Debris shielding at 5600 fps and at normal impact.

Because the quantities r' and C_D, the characteristic debris particle radius and drag coefficient, respectively, are not known accurately, it is convenient to define a new parameter η in which they do not appear

$$\eta = (w/\rho_l)(\rho_s R/\rho r)^{1/2} \tag{14}$$

$$= \eta'[(C_D/2)r/r']^{1/2} \tag{15}$$

In Eq. (6) we can now combine the quantity $(rC_D/2r')^{1/2}$ with the unknown mass loss ratio for the incoming drop G' to yield an unknown dimensionless coefficient B. This results in

$$G = G_o/(1+B\eta) \tag{16}$$

where the second term in the numerator has been neglected as discussed previously. In Eq. (16), G_o and B are considered to be empirical constants which can be determined by testing. These constants are clearly functions of test speed and impact angle and may depend on the test material.

It is worthwhile to note that the debris shielding analysis does not account for the shielding of the body by the aerodynamic shock layer itself. It has been shown[2] that for models of the size generally used in ballistic range tests, the shock layer does not provide shielding against dust particles of order 100 μ in diameter and larger or against precipitation-size water drops, which are of order 1 mm in diameter. We do not know, however, what effect the model shock layer might have on small ice particles, which may occur in rod, platelet, or branched dendritic forms. These particles have high drag and moment coefficients and therefore experience very high linear and angular accelerations. Moreover, these ice particles are relatively fragile (particularly the dendrites) and may be easily shattered, unlike small dust particles or larger raindrops. Thus, while it is reasonable to neglect the shielding effect of the model shock layer upon precipitating raindrops and dust particles, the effect upon ice crystals remains unknown and could possibly be significant. If such shielding occurs, the freestream air density will influence the measured mass loss ratio in a direction opposite to that indicated by Eqs. (14) and (16); that is, a higher air density will provide more aerodynamic shielding and thereby tend to reduce the measured value of G, while at the same time sweeping the debris away more quickly and thereby tending to increase that value.

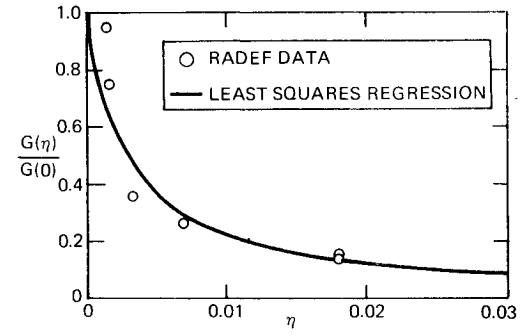

Fig. 3 Debris shielding at 14,000 fps and at normal impact.

A series of tests were conducted in the RADEF to measure debris shielding effects directly by varying the encountered water concentration from 10 to 140 g/m^3 while keeping all other test variables constant. The test model was a $\frac{1}{2}$-in.-diam flat-faced cylinder of a reinforced phenolic. The rain field consisted of 1-mm-diam water drops at 1 atm ambient pressure. The experimental mass loss data were all obtained in tests in which the sample had reached its asymptotic, multiple impact damage limit. The experiments were conducted at two speeds, 5600 and 14,000 fps. The test results, normalized by the empirically determined values of G_o, are shown in Figs. 2 and 3 plotted vs the dimensionless shielding parameter η. The lines in Figs. 2 and 3 represent least squares regressions of the form given in Eq. (16) and provide a satisfactory correlation of the data. The implication of these results is clear: debris shielding can significantly reduce the erosion experienced by a high-speed body, and relatively tenuous particle fields must be employed to obtain realistic erosion data.

References

[1] Reinecke, W., "Rain Erosion at High Speeds," *Proceedings of the Fourth International Congress on Rain Erosion*, Meersburg, Germany, May 1974.

[2] Waldman, G. and Reinecke, W., "Particle Trajectories, Heating, and Breakup in Hypersonic Shock Layers," *AIAA Journal*, Vol. 9, No. 6, June 1971, pp. 1040–1048.

Axisymmetric Buckling of Elastic-Plastic Annular Plates

A. NEEDLEMAN*
MIT, Cambridge, Mass.

I. Introduction

We consider an elastic-plastic annular plate subject to radial in-plane loading at its outer edge. The inner edge of the plate remains traction free and the outer edge the plate is taken to be either simply supported or clamped.

Depending on the thickness of the plate, bifurcation can occur while the plate is in a fully elastic, in a partly plastic, or in a fully plastic state. Attention is focused on cases where bifurcation occurs while the plate is in a partly plastic state and consideration is restricted to axisymmetric bifurcations.

Previous analysis of the buckling of elastic-plastic annular plates have either been of a very approximate character[1] or have employed a stability criterion that was, essentially, a generalization to plates of the reduced modulus theory for columns.[2,3] In this Note, the bifurcation analysis is formulated by means of tangent modulus theory.[4–6] Furthermore, an example is given of the postbuckling behavior and imperfection sensitivity of an annular plate, when bifurcation of the perfect plate takes place from a partly plastic state.

II. Problem Formulation and Numerical Analysis

The inner radius of the annular plate is specified by R_i and the outer radius by R_0. The loading is applied through a monotonically increasing radial compressive displacement U

Received March 14, 1974. This work was partially supported by NSF Grant GP 22796. During the course of this work the author visited the Department of Solid Mechanics, The Technical University of Denmark. Both the support and the hospitality of that department are gratefully acknowledged.

Index category: Structural Stability Analyses.

* Assistant Professor of Applied Mathematics.